Valorization of agro-industrial waste from cotton for production of bio-oil and biochar

Carmem T. Primaz[1,2] Amparo Ribes-Greus[1], Rosângela A. Jacques[2] (*).

[1]Institute of Materials Technology, Universitat Politècnica de València, Camí de Vera, s/n, València, Valencia, 46022, Spain, Phone: +34 630125695

[2]Chemistry Institute, Universidade Federal do Rio Grande do Sul, Av. Bento Gonçalves, 9500, Porto Alegre, Rio Grande do Sul, 91509-900, Brazil, Phone: +55 51 33087213

(*) corresponding author, e-mail and phone:
Rosângela A. Jacques, rosangela.j@iq.ufrgs.br; +55 51 33087213.

ABSTRACT

Cottonseed residue has a high lignocellulosic content, and as such, is a promising candidate for thermochemical techniques that convert biomass into solid, liquid and gaseous fractions, such as pyrolysis. Cottonseed was submitted to fast pyrolysis in a fixed bed reactor and the pyrolysis products were analyzed using several techniques, including elemental analysis, scanning electron microscopy, Fourier-transform infrared spectroscopy, nitrogen adsorption isotherms and two-dimensional gas chromatography. The detailed composition of the bio-oil was investigated using GC×GC/TOFMS combined with software tools, retention indices and dispersion plots. A total of 257 compounds were tentatively identified and 168 were confirmed by LTPRI. The most abundant components of cottonseed products were phenols and nitrogenous

compounds. The amount of nitrogen compounds in the bio-oil distinguishes it from bio-oils produced from other sources of biomass. These compounds may be very useful in the chemical, food, pharmaceutical and biofuel industries. The higher heating values of cottonseed and bio-oil were 19.34 MJ kg $^{-1}$ and 34.25 MJ kg $^{-1}$, respectively, demonstrating the feasibility of the use of cottonseed in its natural form in energy generation or as a secondary source. The biochar had a significant carbon content and a high heating value (22.12 MJ kg $^{-1}$), making it attractive for fuel applications as a substitute for coal. The activation methods used were able to improve the physical and chemical characteristics of the biochar, as demonstrated by methylene blue adsorption tests. The maximum adsorption capacity of NaOH-activated biochar was 23.82 mg g $^{-1}$ while that of K_2CO_3-activated biochar was 332.40 mg g $^{-1}$.The Langmuir isotherm provided the best fit to the experimental data. These results indicate that chemically-activated biochar may be used as an adsorbent in addition to many other applications.

Key Words

Biomass, agro-industrial waste, bio-oil, GC×GC/TOFMS; biochar, chemical activation

1. INTRODUCTION

The use of renewable energy is becoming increasingly imperative to reduce the environmental impact of human activity, economic development and lifestyle changes observed in recent decades. The global energy matrix has suffered changes over time and although biomass does not represent a major contribution to the global energy is expected to play an important role in the global energy balance in the near future. It can be derived from a variety of sources, including but not limited to wood residue, agricultural residue and organic matter from municipal solid waste [1,2]. Biomass can

51 also yield organic and inorganic compounds with high added value through thermal
52 degradation processes such as pyrolysis and liquefaction [3,4].
53 The thermal decomposition of organic substances requires an inert atmosphere
54 (nitrogen or argon) and high temperatures (generally between 400 and 1000 °C), and
55 yields solid (biochar), liquid (bio-oil) and gaseous (non-condensable) products [5,6].
56 Bio-oil is commonly considered as a substitute to petroleum, both in the energy and
57 petrochemical industries and on the other hand, biochar is a carbonaceous material
58 with high density of porous and a large amount of fixed carbon. Its applications are
59 varied and depend on the characteristics of the material itself. Many sources of
60 biomass can be used in the production of bio-oil/biochar. Some of the most
61 advantageous are agro-industrial and domestic waste, which cannot be used for food
62 production like other types of biomass (e.g., oilseeds used to produce biodiesel) [4,7].
63 Cottonseed is an abundant agricultural residue that can be used as raw material in the
64 conversion of biomass into energy and chemical products. The residue from fiber
65 production (seeds) is used in the extraction of vegetable oil, and the remaining seeds
66 are used as animal feed; but these uses are limited by the high fat content (20%) and
67 toxic phenolic compounds present in the seeds [8,9]. As such, cottonseed residue may
68 represent a promising source of clean energy and an alternative to fossil fuels as a
69 primary source of chemical compounds.
70 The use of derived chemical products, bio-oil and biochar establishes a cycle of reuse,
71 where all waste generated by a given process is used to obtain new valuable materials,
72 promoting a zero waste industry. This study provides a complete characterization of
73 cottonseed and its pyrolysis products to encourage the further use of these materials
74 as renewable energy resources.
75

2. MATERIALS AND METHODS

2.1 Pyrolysis of Cottonseed

Cottonseed was obtained from the Planalto Farm, Costa Rica, Mato Grosso do Sul, Brazil. Prior to pyrolysis, the seeds were mechanically pressed to remove excess oil. Fast pyrolysis was conducted using a tube furnace and quartz reactor. Ten grams of cottonseed were used in the experiment, with a (N_2) gas flow of 150 mL min $^{-1}$. The resulting vapors, including the bio-oil, were then passed through an ice-water condenser (with water at T ~-5 °C) to cause partial condensation, with the liquid collected in the collection flask. The sample was heated at 100 °C min $^{-1}$ until the temperature reached 550 °C. The target temperature was maintained for 15 minutes. Mass yield (w/w%) was measured in triplicate, and determined by dividing the weight of the condensate (crude bio-oil) by the initial weight of solid biomass. The crude bio-oil was separated into aqueous and organic phases by liquid–liquid extraction (LLE), using five 5 mL portions of dichloromethane (DCM). After the reactor had cooled, the organic phase was analyzed and the biochar was collected and weighed to determine yield [10].

2.2 Proximate and Elemental Analysis

The moisture, volatile matter and ash content of the cottonseed biomass were determined according to Spanish standard methods UNE-EN ISO (18134-1/18134-2/18134-3:2015), UNE-ISO 18123:2015, UNE-EN ISO 18122:2015, respectively, and fixed carbon was determined by mass difference. Elemental analysis was performed on samples of biomass, bio-oil and biochar (activated and non-activated) using a CE Instruments CHNS1100 device to determine the percentage of carbon, nitrogen, hydrogen and sulfur in the samples.

100 The higher heating value (HHV) for the bio-oil was measured using a bomb calorimeter
101 (IKA Werke model C5003) in accordance with ASTM D240.

102 **2.3 Thermal gravimetric analysis**

103 Thermal gravimetric analysis (TGA) was performed using a Mettler Toledo TGA/SDTA
104 851 (Columbus OH) analyzer, heating the sample from 25 °C to 900 °C at 10°C min^{-1}
105 under an inert atmosphere (ultra-pure nitrogen at 25 mL min^{-1}).

106 **2.4 Infrared Spectroscopy (FTIR)**

107 FTIR was performed using a Cary 630 FTIR-ATR spectrometer (Agilent Technologies).
108 The samples were scanned over a wide range (400 cm^{-1} to 4000 cm^{-1}) for a total of
109 64 scans at a resolution of 4 cm^{-1}.

110 **2.5 Scanning Electron Microscope (SEM)**

111 The analyses were performed using a scanning electron microscope with a field
112 emission gun (FEG) (HITACHI, S-4800) at an acceleration voltage of 10 kV and
113 magnifications ranging from 100x to 6000x.

114 **2.6 Obtaining the N_2 - BET Adsorption Isotherms**

115 The physical characteristics of the biochar surface were examined using the BET
116 method (Brunauer, Emmett and Teller) and the micropore size distribution was
117 determined using density functional theory (DFT) [11,12]. Prior to evaluating the
118 adsorption isotherms, 50 mg of the sample were degassed for 30h at room temperature
119 in a vacuum chamber. Nitrogen adsorption and desorption isotherms were then
120 measured at the boiling temperature of nitrogen using a Micromeritics Tristar II Kr 3020
121 surface analyzer (Micromeritics, Germany).

122

2.7 Determination of pH at the point of zero charge (pH_{PZC})

For each material, a curve was obtained by plotting the pH of the equilibrium solution as a function of the solid mass fraction. The pH at the point of zero charge (pH_{PZC}) of the materials was determined throw the measure of the pH value of the suspension with the highest solid fraction when pH evolution with solid concentration is low; that is, the plateau in the plot of equilibrium pH versus solid weight fraction corresponds to the pH_{PZC} of the sample. pH_{PZC} was determined according to the method proposed by Noh and Schwarz [13] with the modifications proposed by Reymond and Kolenda [14]. Measurements were performed using a HACH Sension^{+} PH1 DL Portable pH meter (GB-Manchester) using 100 mg of the dry sample (biochar) divided into 5 glass vials (20 ml), to which appropriate amounts of Milli-Q water were added to achieve mass ratios of 10, 8, 6, 4, and 2% of biochar to water. Samples were kept under continuous agitation at a constant temperature of 25 °C. pH was measured after 24 h of contact to ensure all samples had enough time to reach pH equilibrium.

2.8 Chemical activation of biochar

The chemical activation of cottonseed biochar was carried out using two different processes in order to compare their relative effectiveness.

2.8.1 Activation with alkaline solution (NaOH)

Activation with sodium hydroxide was performed using the method proposed by Jin et al., [15]. The process was performed by adding 2 g of biochar to 500 mL 2 mol L^{-1} sodium hydroxide solution (NaOH, 99 % purity, Sigma Aldrich, Seelze/Germany) kept under stirring for 2 h. The suspension was then filtered and the material recovered with filter paper. After filtration the samples were washed with deionized water and the

suspension was stirred several times until the pH of the filtrate remained stable. The material was then filtered and dried for 12 h in an oven at 105 °C.

2.8.2 Activation with Potassium Carbonate (K_2CO_3) in inert atmosphere

This process was performed according to the methodology proposed by Maciel et al., [16] with some modifications. Briefly, the biochar was placed in contact with the activator (K_2CO_3, 99 % pure, Sigma Aldrich, Seelze/Germany) at a biochar/carbonate mass ratio of 1:3 in a porcelain capsule. The mixture in the capsule was then introduced into a horizontal tubular stainless-steel reactor. The reactor temperature was raised by 10°C min^{-1} until a target temperature of 800 °C was reached. The temperature was maintained for 2 hours, with continuous flow of nitrogen gas at a rate of 5 mL s^{-1}.

2.9 Methylene blue adsorption tests

Prior to evaluating the adsorption of activated and non-activated biochar, kinetic experiments were used to determine time of equilibrium. After the activation process, biochar can exhibit different behaviors as a function of adsorbate/adsorbent contact time, concentration and amount of adsorbent, especially after K_2CO_3 activation. As a result, the parameters used for the kinetic models were different for each biochar activation processes.

Activated biochar was left in contact with 4 mL of methylene blue dye solution at concentrations ranging from 10 to 450 mg L^{-1} (details for each activation process are described in the subsequent section). Methylene blue solutions were prepared by diluting the stock solution in distilled water prior to each adsorption test.

Tests were performed in 5 mL screw-cap glass vials covered with aluminum foil to prevent photodegradation. The samples were placed on a Heidolph shaker under

constant stirring at 700 rpm at room temperature (25 °C), for periods ranging from 30 min to 24h depending on the material.

The samples were then centrifuged and the concentration of the remaining adsorbate (methylene blue dye) was determined using a UV-Vis spectrophotometer (Cary-60, Agilent Technologies) at a wavelength of 665 nm, which corresponds to the is wavelength of peak absorption for the methylene blue dye. After measurements were taken, the concentration was calculated using the calibration curve (0 to 10 mg L^{-1}) of methylene blue according to the Lambert-Beer law.

Kinetic study: 5 mg of K_2CO_3-activated biochar and 10 mg each of non-activated and NaOH-activated biochar were used in this experiment. The following parameters were defined for each material:

a) For non-activated and NaOH-activated biochar, concentrations of 10, 35, 45 mg L^{-1} were used, and samples were collected at 60, 120, 240, 300, 720 and 1440 min.

b) For inert atmosphere (N_2) and potassium carbonate-activated biochar, concentrations of 350, 400, 450 mg L^{-1} were used and samples were collected at 30, 60, 90, 120, 150, 180, 380 and 480 min.

Equilibrium study: the study of equilibrium adsorption isotherms was conducted according to the results of kinetic studies, after enough time of contact had passed, for the biochar and methylene blue solutions to reach equilibrium.

For non-activated and NaOH-activated biochar, solutions with concentrations of 15, 25, 35, 45, 55 and 75 mg L^{-1} were stirred at 700 rpm for 720 min (selected equilibrium time determined from the kinetic studies). For K_2CO_3-activated biochar, the concentrations used were 250, 300, 350, 400 and 450, and the equilibrium time was 180 min. Residual adsorbate concentrations for each material were also analyzed by UV-Vis spectrophotometer.

The maximum adsorption capacity was calculated using **Equation (1)**, with the concentration calculated after equilibrium time. These results were adjusted to Langmuir model using **Equation (2),** and the Freundlich model using **Equation (3),** [17]**.**

$$Q_e = \frac{(C_0 - C_e)V}{m} \quad (1)$$

$$Q_e = \frac{Q_0 K_L C_e}{1 + K_L + C_e} \quad (2)$$

$$\frac{Ce}{Qe} = \frac{1}{K_L Q_0} + \frac{Ce}{Q_0} \quad (3)$$

2.10 Analysis of bio-oil by GC×GC/TOFMS

Bio-oil samples were analyzed using a GC × GC system (Agilent Technologies, Palo Alto, CA, EUA) coupled to a Pegasus IV (Leco, St. Joseph, MI, USA) time-of-flight mass spectrometer. The analysis was performed on a 60 m, 250 µm i.d. DB-5 (95% dimethylpolysiloxane and 5 % phenyl groups) capillary column with 0.25 µm film thickness and a 2.5m, 180 µm i.d. a DB-17-ms (50 % phenyl and 50 % dimethylpolysiloxane) column with 0.18 µm film thickness. Both were purchased from J & W Scientific (Folsom, CA, USA).

After optimization, the parameters used for these analyses were as follows: 280 °C injector and ion source temperature; 1 µL splitless injection volume and 10 mg mL^{-1} sample concentration. Oven heating started at 60 °C for 1 min, and increased to 280 °C at a rate of 3 °C min^{-1}. A second oven was kept at 5 °C above the first. The carrier gas was helium at a flow rate of 1 mL min^{-1}. The modulation period was 8 s with a 0.6 s hot pulse.

The mass spectrometer operated in a range of 45–400 Da and recorded 100 scans per second (100 Hz). The retention index (LTPRI) for each compound was calculated according to Van den Dool & Kratz [18] based on the retention times of a standard mixture of linear n-alkanes (C_6-C_{30}). The experimental retention index was then compared with data from the NIST Mass Spectral Library.

The concentration of peaks was estimated based on the analysis of relative peak areas. Each compound in the bio-oil was evaluated according to its functional group and family, allowing for the tentative identification of all chemical classes present in bio-oil, though the response factor of each compound was not taken into account. Nevertheless, considering the large number of compounds identified and the impossibility of obtaining analytical standards for each compound, this procedure can be used to estimate the percent area of major peaks, to compare different samples and screen for possible changes. Further details on this approach are described elsewhere [10,19–21].

3. RESULTS AND DISCUSSION

The original biomass and the products of the pyrolysis (bio-oil and biochar-activated and non-activated) were analyzed and characterized by several techniques. The results and discussion for the Thermal gravimetric analysis, Proximate and Elemental analysis, Infrared Spectroscopy (FTIR), Scanning Electron Microscope (SEM), N_2-BET Adsorption Isotherms and Determination of pH at the point of zero charge (pH_{PZC}) can be viewed in the **Supplementary Material Part A**.

3.1 Thermal gravimetric analysis

The cottonseed demonstrated a high content of volatile and semi-volatile matter (~75 %), indicating that thermal degradation may be an effective method of extracting

compounds of interest from this type of biomass. The deconvolution of the derivative (DTG) curve helped define the temperature ranges with the highest percentage of mass loss for each of the main components of the cottonseed (cellulose, hemicellulose and lignin).

3.2 Pyrolysis of cotton seed

The mass yields of the products obtained in cottonseed pyrolysis process were calculated as shown in **Figure 1**.

Figure 1: Effects of temperature on yields of cottonseed pyrolysis products.

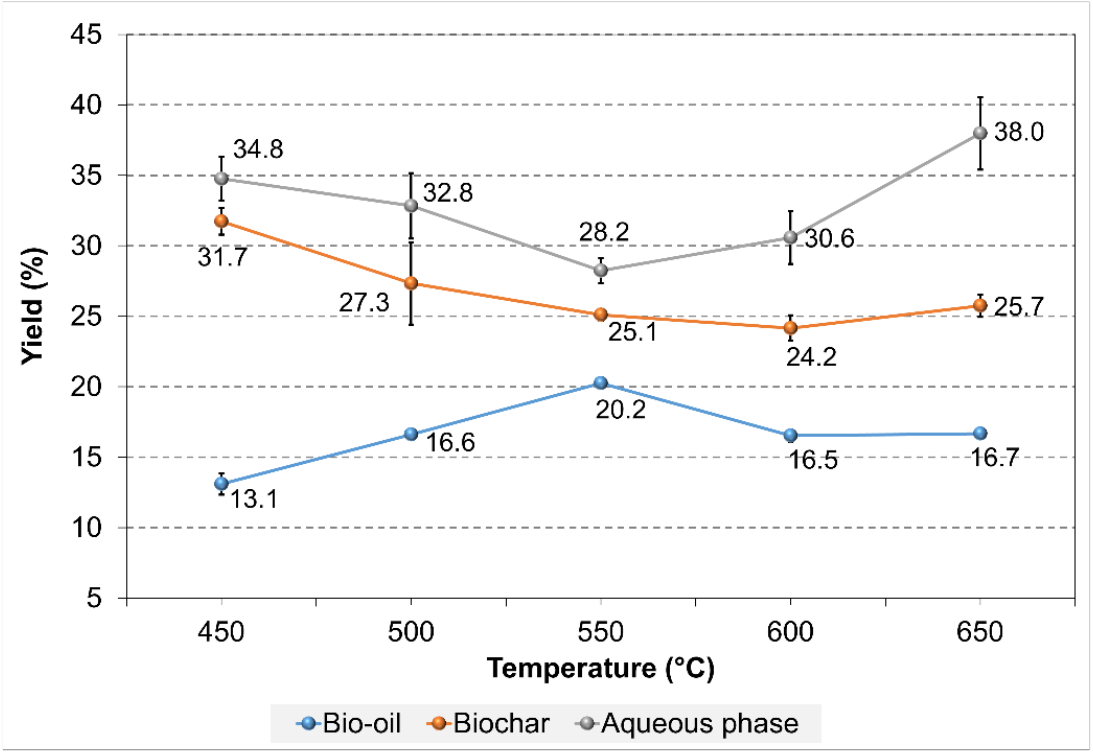

The maximum bio-oil yield of 20 % was obtained at 550 °C. Above this temperature, the bio-oil yield decreased to approximately 16 %. This can be predominantly attributed to secondary reactions (breakdown and rearrangement) of pyrolysis vapors at high temperatures [22,23].

253 Previous studies of cottonseed biomass do not separate the aqueous phase from the
254 bio-oil as was done in this study, and refer to the entire liquid fraction as bio-oil,
255 resulting in much higher yields than observed in this paper. The application of this
256 approach to the present findings would result in crude bio-oil (including the aqueous
257 phase) yields of 48 % (at 450 °C), 49 % (at 500 °C), 48 % (at 550 °C), 47 % (at 600
258 °C) and 55 % (at 650 °C). These values are in line with previous literature, but as they
259 include large amounts of water, they are only useful for comparison purposes [24–26].
260 Apaydin-Varol et al., [25] performed the fast pyrolysis of cottonseed in order to define
261 process variables such as temperature (400 – 700 °C), heating rate (5 – 700 °C min $^{-1}$)
262 and nitrogen flow rate (100 - 800 cm ^{3} min $^{-1}$); the maximum bio-oil yield obtained by
263 these authors was ~ 49 % at a temperature of 500 °C under a nitrogen flow of 200 cm^{3}
264 min $^{-1}$ and a heating rate of 300 °C min $^{-1}$.
265 According to several authors, maximum bio-oil yield occurs between 350 and 500 °C
266 since pyrolysis reactions occur at different temperatures, supporting the hypothesis
267 that higher temperatures cause the decomposition of molecules in the solid state,
268 producing smaller molecules and a subsequent increase in gas yield [2,24].
269 Biochar yield decreased from 32 % to 24.2 % when the temperature increased from
270 450 °C to 650 °C. This reflects the severe decomposition of organic molecules at higher
271 temperatures, increasing the yield of gaseous product at the expense of the biochar
272 ratio [22,27]. Similar observations of higher biochar yields at lower temperature have
273 been recorded by other researchers for various types of biomass [28], including
274 crambe seeds [29], spent coffee grounds [27], sorghum [30], cotton stalk [26] and wood
275 [31].
276 At higher temperatures, the gas yield increases due to the secondary reactions of
277 pyrolysis vapors within the reactor, while the decrease in char yield decreased is

attributed to the primary decomposition of the feedstock and the secondary decomposition of char at higher temperatures. During secondary decomposition, non-condensable gas products also contribute to the elevated gas yields which occur with increasing temperature [5,24].

The aqueous fraction of pyrolysis oil comes from the moisture in the biomass and the dehydration of organic compounds (especially cellulose and hemicellulose) during the pyrolysis process [5,32]. The main degradation products of cellulose and hemicellulose are water-soluble. A fraction of the water yield forms a separate aqueous phase while the rest is dispersed into oil. The water-insoluble fraction of the oil consists mainly of lignin-derived materials. The recovery of organic compounds from the aqueous phase may be of interest as a potential source of hydrogen, alkanes and polyols [33,34]. The water content of the bio-oil ranged from approximately 28 to 38 %, and was highest at 650 °C.

Longer residence times in the pyrolysis reactor can lead to further breakdown (dehydration, decarboxylation and condensation) of these compounds, increasing the production of water and non-condensable with smaller molecules such as carbonyls and aliphatic hydrocarbons [5,23] affecting the yield and promoting repolymerization reactions. A short residence time favors the formation of liquid products (bio-oil) since the rapid passage of organic vapors through the reactor minimizes side reactions and preserves the fatty acids and esters in the bio-oil [22,23].

The results showed that the reaction temperature significantly affected the yield of pyrolysis products. The highest yields recorded were ~ 20 % for bio-oil at 550 °C and ~ 32% for biochar at 450 °C.

3.3 Analysis by Infrared Spectroscopy (FTIR)

This analysis confirmed the efficiency of the project by comparing the FTIR of the solids before and after and the pyrolysis with the complete withdrawn of organic compounds from the biomass. On the other hand, the bio-oil shows typical absorptions of OH, COOH, COOR, =CO and alkyl and aromatic chains.

3.4 Scanning Electron Microscope (SEM)

The results for this characterization allow the best visualization and demonstrated the efficiency of the applied activation methods, especially with K_2CO_3 that allowed for the development of a larger surface area for the biochar.

3.5 N_2 - BET adsorption isotherms

These results suggest that the pyrolytic process used in the present study, along with chemical activation with potassium carbonate, allow for the production of porous material from residual cottonseed.

3.6 Determination of pH at the point of zero charge (pH_{PZC})

The results of pH_{PZC} measurements of activated biochars suggested that the surface of these materials possesses basic characteristics that may aid in the adsorption of the methylene blue cationic dye in aqueous solutions; adsorption can be favored by ensuring that the solution pH is above 7.

3.7 Dye adsorption tests: Methylene blue as adsorbate for activated biochars

3.7.1 Adsorption kinetics

Contact time is an important parameter for determining the equilibrium time and kinetics of the adsorption process. The kinetics of an adsorption system describes the rate of solute adsorption, which determines the required residence time for adsorption

to occur at the solid-liquid interface. Kinetic studies showed that the equilibrium and maximum adsorption time differed between the materials examined.

Adsorption kinetics were investigated at room temperature, in varying concentrations (from 10 to 450 mg L^{-1}) of methylene blue dye. Adsorption time curves are shown in **Figure 2 (a, b, c)**.

Figure 2: Kinetic curve with percentage of methylene blue removal as a function of contact time for (a) non-activated biochar and (b) NaOH-activated biochar at concentrations of 10, 35 and 45 mg L^{-1} and for (c) K_2CO_3-activated biochar at concentrations of 350, 400 and 450 mg L^{-1}. The other conditions used for these experiments are described in experimental section.

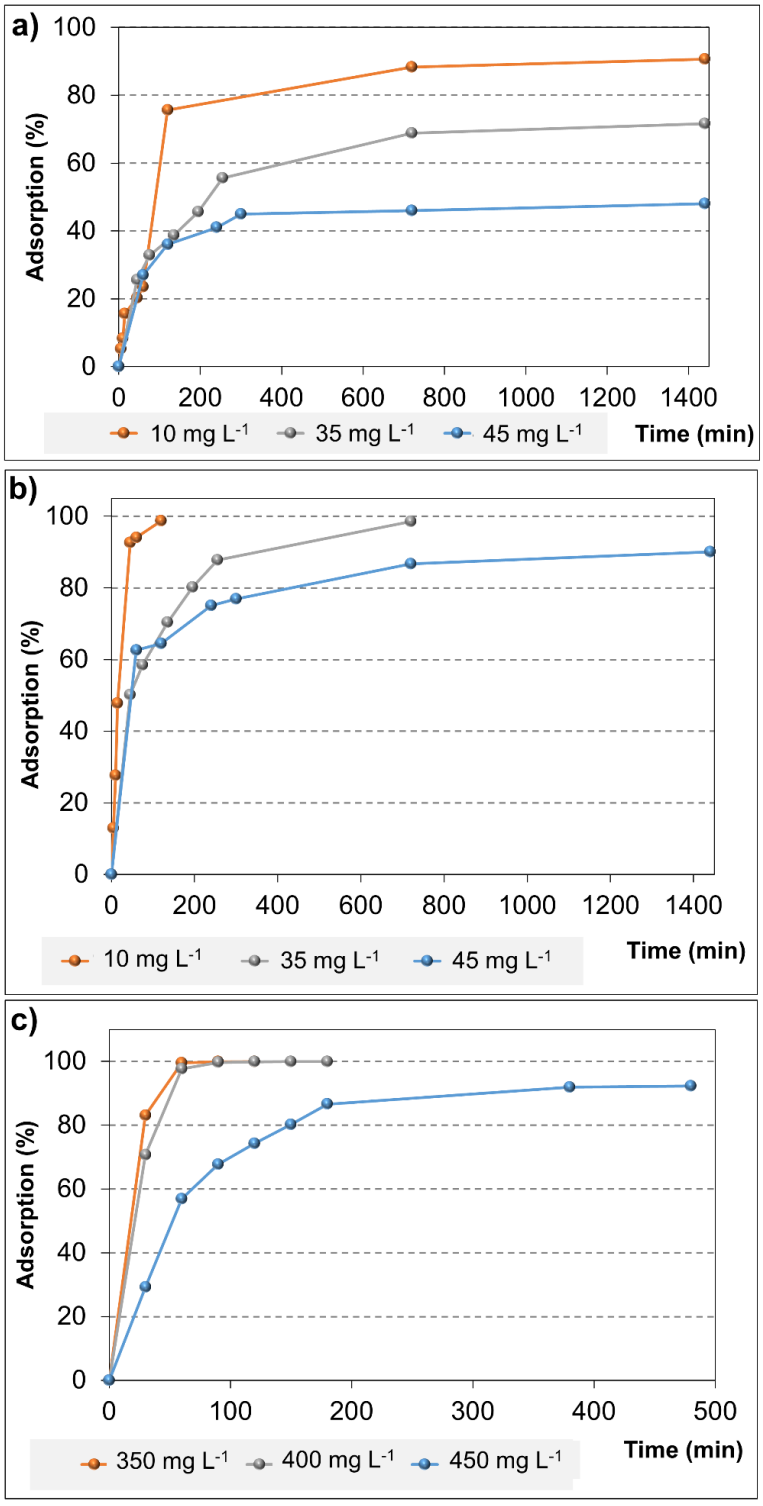

335 The kinetic analysis of non-activated biochar **(Figure 2-a)** showed that the system
336 reached equilibrium in approximately 300 minutes. However, the material had a very
337 low dye adsorption capacity. At 300 min, the adsorption percentages at concentrations
338 of 35 and 45 mg L^{-1} were 68.65% and 46.71 %, respectively, while in the solution with
339 the lowest concentration (10 mg L^{-1}), 88.63% of the dye was adsorbed.
340 For NaOH-activated biochar **(Figure 2-b),** the adsorption process reached equilibrium
341 in approximately 720 minutes. At this time, 95.55% and 86.71% of the dye had been
342 removed at concentrations of 35 and 45 mg L^{-1}. In the solution with the lowest
343 concentration (10 mg L^{-1}), 99.63% of the dye was removed after in 120 minutes.
344 The kinetic studies of K_2CO_3- activated biochar **(Figure 2-c)** revealed that the system
345 with the most concentrated solution (450 mg L^{-1}) reached equilibrium in 180 minutes
346 after which approximately 87% of the dye was adsorbed. This percentage remained
347 stable for the remainder of the test period. In solutions with concentrations of 350 and
348 400 mg L^{-1}, the highest concentration decrease occurs after 60 minutes of contact, and
349 was measured to be 99.55% and 97.69%, respectively. At initial contact, far from the
350 point of equilibrium, kinetics are governed by the rate of reactions on the adsorbent
351 surface; when the system approaches equilibrium, the predominant surface kinetics
352 mechanism shifts to intraparticle diffusion [35].

353 **3.7.2 Adsorption isotherms**

354 Adsorption isotherms provide important information about the adsorption process,
355 such as the ratio of adsorbate per unit mass of adsorbent to the distribution of
356 adsorbate molecules at the solid/liquid interface when the system reaches equilibrium.
357 Additionally, isotherms indicate how the adsorbent will effectively interact with the
358 adsorbate and whether the desired process is feasible. As such, the analysis of

isothermal data and its adjustment it to different models is an important step toward the identification of a suitable adsorption mode [36,37].

The adsorption capacity of non-activated and activated biochar was tested in the time interval determined in the kinetic studies. Non-activated and NaOH-activated biochar were tested for a period of 720 minutes, while K_2CO_3-activated biochar was tested for 180 minutes. Assays were performed with a concentration within the equipment detection range and the experiment was conducted at 25 °C.

As observed in the kinetic studies, the amount of adsorbate increased with increasing solute concentration in the liquid phase, and the adsorbate distribution between the two phases represented adsorption equilibrium. This equilibrium is usually represented by the amount of solute adsorbed per unit mass of the adsorbent as a function of the concentration of solute in the equilibrium solution [38,39].

After the equilibrium data were obtained, it was adjusted to the non-linear isotherm models of Langmuir and Freundlich. **Figure 3 (a-c)** shows the adsorption isotherms along with the adjusted curves for biochar activated with alkaline solution, while **Table 1** presents the constants obtained in the adjustment to each mathematical model.

Table 1: Constants obtained for the maximum adsorption capacity of the cottonseed biochar non-activated and activated, adjusted to the mathematical models of Langmuir and Freundlich using as adsorbate the methylene blue dye.

Cotton seed biochar	Constants of Langmuir				Constants of Freudlich		
	K_L(L mg^{-1})	Q_0(mg g^{-1})	R_L	R^2	n	K_F(mg g^{-1})	R^2
Non-activated	0.35	7.82	0.17	0.99	1.42	5.29	0,93
Activated with NaOH	0.85	24.87	0.01	0.98	3.38	11.15	0.89
Activated with K_2CO_3	3.75	333.30	5.92×10^{-4}	0.99	11.70	254.74	0.94

379 The amount of methylene blue adsorbed until the equilibrium time was reached ranged
380 from **2.76** to **9.56** mg g $^{-1}$ for non-activated biochar at concentrations of 15 to 75 mg L
381 $^{-1}$, while alkaline activated biochar adsorbed **5.89** to **23.82** mg g $^{-1}$ of dye under the
382 same time and concentration conditions.
383 The highest adsorption capacity was obtained for K_2CO_3-activated biochar, which
384 increased from **199.90** mg g $^{-1}$ to **332.40** mg g $^{-1}$ as concentration went from 250 to 450
385 mg L $^{-1}$. The rise in adsorption capacity with increased initial concentration is mainly
386 due to the higher number of available molecules for adsorption, but may also be
387 attributed to an increase in mass transfer, promoting greater interaction between
388 adsorbent and dye molecules [40,41].
389 The isotherms obtained for K_2CO_3-activated biochar **(Figure 3-b)** demonstrate high
390 affinity to the dye and favorable adsorption capacity, with adsorption occurring rapidly
391 and the dye remaining bound to the adsorbent until equilibrium was reached.
392 The Langmuir model provided the best fit to the experimental data for both activated
393 materials, as can be seen in **Table 1.** The adjustment was confirmed by R^2 values.
394 This model is assuming that the adsorption process takes place on a homogeneous
395 surface with monolayer adsorption (the atom or molecule of the adsorbent binds to
396 specific sites on the surface of the adsorbent).
397 The efficiency of the adsorption process, predicted by the dimensionless equilibrium
398 parameter R_L, provides further evidence of the satisfactory adsorption properties of
399 activated biochars. The adsorption nature is considered unfavorable if $R_L > 1$, linear if
400 $R_L = 1$, and favorable if $0 < R_L < 1$. As can be observed in **Table 1**, non-activated biochar
401 had an R_L value of 0.17, while NaOH- and K_2CO_3-activated biochar had values of
402 0.01 and 5.92 $\times 10^{-4}$, respectively [42,43].
403

404

405 **Figure 3**: Adsorption isotherms construct at 25 °C for (a) non-activated biochar and (b) NaOH-
406 activated biochar after 720 minutes of contact and for (c) K_2CO_3-activated biochar after 180 minutes
407 in contact with methylene blue solutions in different concentrations (Q_{eq} = adsorbed amount and
408 C_{eq} = equilibrium concentration).

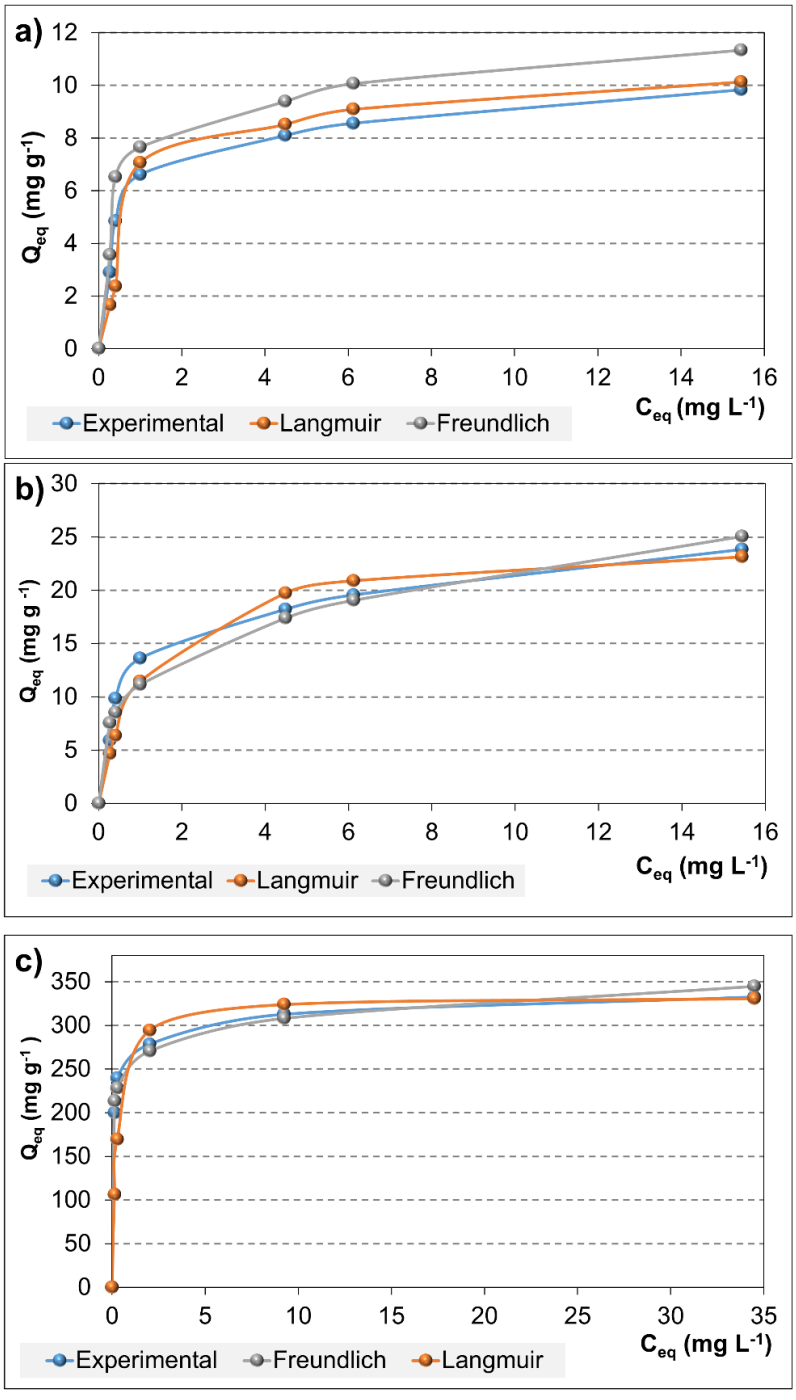

409

The Langmuir (K_L) constant refers to the amount of substance adsorbed per unit mass of adsorbent at equilibrium. This value was higher for K_2CO_3-activated biochar than non-activated and NaOH-activated samples, which points to greater interaction between the dye and the surface of K_2CO_3-activated biochar relative to the other samples [17].

The Freundlich constant (K_F) is related to adsorption capacity. However, unlike the Langmuir constant Q_0, K_F does not inform the maximum removal capacity, since the Freundlich model does not predict surface saturation [36,43].

The constants obtained for the Freundlich model were also analyzed. This model assumes that adsorption occurs on a heterogeneous layer, and includes a parameter (n) which represents surface heterogeneity and adsorption intensity. When n=1, adsorption is linear, while n < 1 suggests that the adsorption process is chemical, while n > 1 indicates physical adsorption.

In the present study, non-activated biochar had an *n* value of 1.42, while the *n* value of NaOH-activated biochar was 3.38, and that of K_2CO_3-activated biochar, 11.70. These values are indicative of favorable adsorption, and are compatible with previous literature on methylene blue adsorption, where studies report values in the 1-10 range [44,45]. The parameter *1/n* indicates the intensity of adsorption and the degree of surface heterogeneity, where values near zero are indicative of more heterogeneous surfaces. The 1/n values for non-activated, NaOH-activated and K_2CO_3-activated biochar were 0.70, 0.29 and 0.08 respectively. These values provide further evidence that the isotherms were favorable, though the Freundlich model was not the best fit to the data.

Once the experimental data were fitted to the Langmuir isotherm, the values obtained for the Q_o parameter, which describes the monolayer saturation capacity of the

435 adsorbent, were 7.82 mg g^{-1} for non-activated biochar, 24.87 mg g^{-1} for NaOH-
436 activated samples and 333.30 mg g^{-1} for K_2CO_3-activated biochar.
437 These findings together with the initial characterization of these materials suggest that
438 NaOH activation resulted in basic functional groups on the biochar surface, which
439 enabled methylene blue, a cationic dye, to interact with the material through negatively
440 charged active sites.
441 Previous studies using this technique [46–48], found that alkaline-activated biochar
442 showed efficient removal of methylene blue dye, though the largest differences in
443 maximum adsorption capacity were obtained for K_2CO_3-activated biochar, whose
444 surface had a higher and more ordered pore density develop during activation at high
445 temperatures and, according to characterization results, presented basic functional
446 groups that interacted with the cationic dye and facilitated the access of molecules to
447 the inside of the pores.
448 These results suggest that intrinsic characteristics such as total surface area and larger
449 pore volumes play a very important role in the dye removal process. The values
450 obtained in the present study were very promising, since they are close to the
451 maximum adsorption capacity of methylene blue by commercial activated charcoal,
452 which is 388 mg g^{-1}, according to the Langmuir model [49,50].
453 The maximum adsorption capacity of K_2CO_3-activated cottonseed biochar observed in
454 this study using methylene blue was also higher than that of many other adsorbents
455 described in the literature.
456 Recently, T. Sarat Chandra et al., [39] investigated the use of defatted algal biomass
457 (DAB) as a non-conventional low cost adsorbent and found the raw, defatted and
458 pretreated DAB had maximum adsorption capacities of 6.0, 7.73 and 7.80 mg g^{-1},
459 respectively.

460 A. Nasrullah et al., [40] prepared activated carbon-alginate (AC-alginate) beads by
461 entrapping activated carbon powder from mangosteen fruit peel into calcium-alginate
462 beads, and tested their efficacy at removing methylene blue dye from an aqueous
463 solution. The results showed that the beads had a maximum adsorption capacity of
464 230 mg g^{-1}. Foo and Hameed [51], prepared activated carbon from date seeds using
465 microwave-assisted KOH activation and obtained an adsorption capacity of 316.11 mg
466 g^{-1} for methylene blue.
467 There are no reports of production and activation of cottonseed biochar for use as an
468 adsorbent. Previous studies of this material focused on the production of biochar from
469 cotton stalks. In a study by Deng et al. [52], cotton stalks were chemically activated
470 with KOH (KAc) and K_2CO_3 (KCAc) under microwave irradiation and tested for
471 methylene blue adsorption. Adsorption equilibrium data for both activated carbons
472 were best fitted to the Langmuir isotherm. The maximum adsorption capacities of KAc
473 and KCAc were 294.12 mg g^{-1} and 285.71 mg g^{-1}, respectively.
474 The data showed that the activation processes used in the present study were effective
475 at improving the adsorption capacity of biochar for methylene blue dye, especially in
476 the case of K_2CO_3 activation.
477 However, the differences in adsorption capacity of the materials indicated that the
478 adsorption of organic compounds by carbonaceous materials depends on the physical
479 and chemical properties of biochar. The pore structure influences physical adsorption,
480 with surface area and pore volume emerging as the most important factors. However,
481 the surface chemistry of the materials also has a major effect on the adsorption of
482 organic compounds, through its influence on surface charge, electron density and
483 hydrophilicity.
484

3.8 Analysis of bio-oil by GC×GC/TOFMS

The chromatographic profile of cottonseed bio-oil analyzed by GC×GC/TOFMS can be seen in the two-dimensional diagram in **Figure 4.**

The sample has a complex profile, and the presence of large amounts of oxygenated compounds with very close retention times in a specific region of the chromatogram requires a highly efficient separation technique.

Figure 4: Two-dimensional color diagram (GC×GC/TOFMS) of the organic fraction of the cottonseed bio-oil.

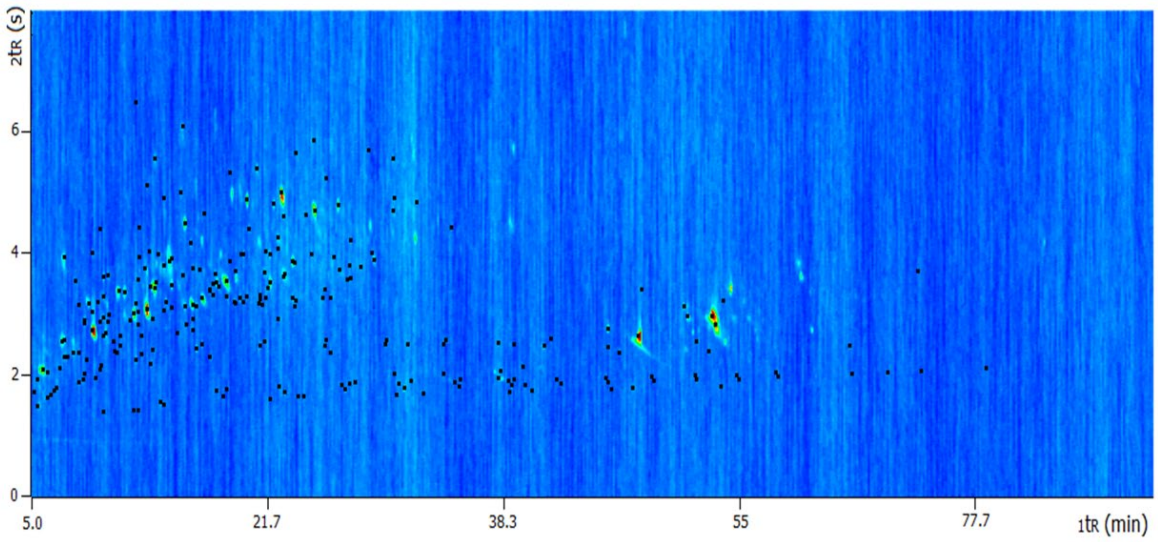

A total of 257 compounds were tentatively identified in the cottonseed bio-oil, and 168 were confirmed by linear temperature programmed retention indices (LTPRI), with good agreement (within a range of ± 20) between calculated values and those in the NIST library. The use of LTPRI allowed for the identification of compounds with greater reliability.

The list of compounds identified by GC×GC/TOFMS is presented in **Table B1 (Supplementary Material)** and includes the components for which LTPRI values were not located in the literature. These compounds were tentatively identified by comparing

502 the mass spectra with the equipment database and the locations of peaks in dispersion
503 profiles.

504 The following classes of compounds were identified in the cottonseed bio-oil: nitrogen
505 compounds (56 compounds), phenols (42 compounds), hydrocarbons (90
506 compounds), acids (10 compounds) and ketones (24 compounds). The comparison of
507 relative peak areas revealed that the most abundant compounds in the bio-oil sample
508 were phenol (9.2%), 3-methyl phenol (5.2%) and Indol (4.7%). The yield from
509 mechanical extraction of cottonseed oil is, on average, 17-24%; this value is
510 considered low relative to other raw materials such as canola, sunflower and castor
511 bean, whose oil yield ranges from 30 to 50% [8,9]. The cotton oil transesterification
512 has generated significant interest, however this method involves mainly of extraction,
513 methanolysis and purification, which are time consuming and require expensive
514 chemicals [25]. Fast pyrolysis is a single-step thermochemical conversion method,
515 which is also less expensive than other techniques, making it an attractive alternative
516 for the production of fuel products. **Figure 5-c** shows the major compounds
517 (concentration > 1 %) found in the bio-oil.

518

Figure 5: Distribution of classes of compounds in the bio-oil of pyrolysis of CS at 550 °C, sorted according to the relative percent area (a) number of compounds (b) and (c) major compounds (conc. % > 1.0 %).

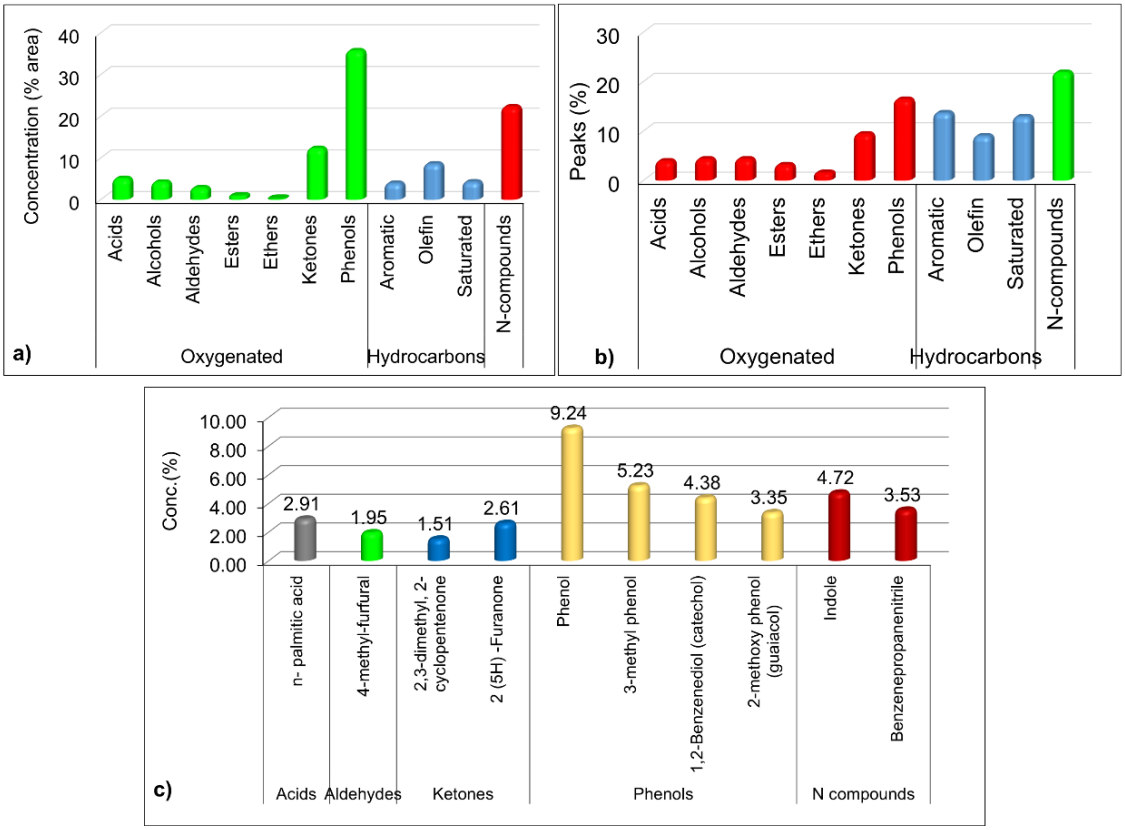

The analysis of relative areas showed that there is no direct relationship between the number of peaks in each class and the area occupied by them. This is especially clear in the case of hydrocarbons and acids. However, for oxygenated compounds such as phenols and ketones, as well as nitrogenous ones, total area is more evenly distributed among the peaks. This is most evident in **Figure 5 (a, b)**, which compares the relative peak area (total percentage area occupied by the compounds in each class) between qualitatively identified hydrocarbons, phenols, ketones and other compounds (number of peaks present in each class)

3.9 Dispersion Plots

Dispersion plots illustrate the spatial distribution of different compounds according to molecular weight, number of substituents and number of branches. In a complex sample, compounds with similar structures elute in the same areas of the two-dimensional space, allowing for an analysis of the spatial distribution of chemical classes. This method sheds light on the global composition of bio-oil and contributes to qualitative analysis. Dispersion curves were plotted on Microsoft Excel™ using the retention times for each identified peak. The use of dispersion curves facilitates the analysis of spatial distributions, as observed in previous studies conducted by our research group [20,53].

Figure 6 (a-d) shows the spatial distribution of chemical classes in the bio-oil sample. A clear distribution trend for some chemical subclasses can be observed in the 2D separation space.

Figure 6. Dispersion Graphics for the chemical classes on the organic fractions of the bio-oil from cotton seed: (a) oxygenated compounds; (b) phenols; (c) N-compounds; (d) hydrocarbons (e) acids and esters.

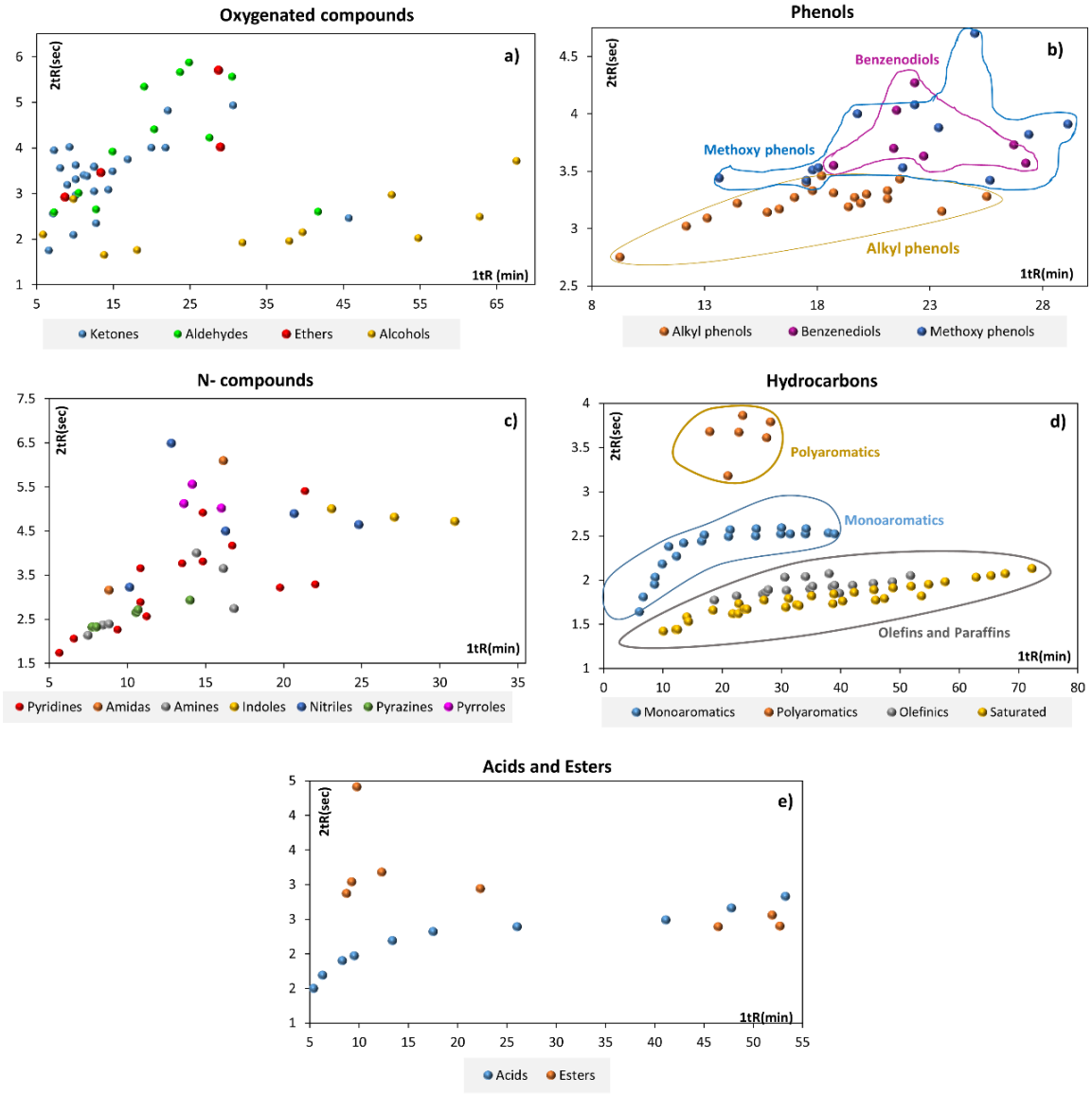

Some phenols, ketones, aldehydes and nitrogen compounds show a clear separation in the 2D due to significant polarity differences, while acids, esters and hydrocarbons demonstrated efficient separation in the 1D.

Phenolic subclasses **(Figure 6 (b))** (alkyl, methoxy and benzenediols) can be seen in different parts of the separation space. Alkyl phenols are distributed according to the

554 number of carbons in the side chain (from phenol C_0 to phenols with 1, 2 and 3 carbons
555 in the side chain). Methoxy phenols and benzenediols have longer elution times in the
556 second dimension as a result of their high polarity relative to alkyl phenols.
557 Phenolic compounds, mainly derived from lignin degradation [2,54], are some of the
558 most abundant in bio-oil. This class of compounds has great importance and is widely
559 used for industrial purposes. As such, cottonseed bio-oil appears to be an
560 economically viable source of phenols.
561 As for the applications of the identified compounds, phenol may be of great importance
562 as a substitute for petrochemical phenol in the production of phenolic resins (phenol-
563 formaldehyde) in the electronic and wood treatment industries. Some studies report
564 that up to 50% of phenols can be replaced bio-oil equivalents with no damage to the
565 quality of the resin [54,55].
566 As expected, the spatial arrangement of hydrocarbons was determined by the number
567 of carbons in the side chain, as can be seen in **Figure 6 (d).** The separation of
568 hydrocarbons occurs mainly in the first dimension, and is also related to the increase
569 of carbon atoms in the chain. Paraffins have carbon chains from C_{10} to C_{29}, much like
570 olefins and monoaromatics. Polyaromatic hydrocarbons have longer elution times in
571 the second dimension (3.8 and 5.3 s).
572 The separation of carboxylic acids and esters **Figure 6 (e),** occurs mainly in 1D due to
573 their volatility, but the presence of these compounds was not as evident in this bio-oil
574 sample. The significant decrease in oxygen content of bio-oil compared with the
575 original feedstock is important. This decrease was confirmed by elemental analysis of
576 the raw material and the bio-oil produced [55].
577 The composition of cottonseed bio-oil was distinct from that of bio-oils produced from
578 different biomasses [56], such as spent coffee grounds [10], mango seed [53], rice

husk and peach pit [57]. This peculiar characteristic is the richness of nitrogen compounds. The main distinguishing feature of cottonseed bio-oil was the abundance of nitrogen compounds. Proteins account for up to ~25% of cottonseed weight, and the presence of protein results in a higher content of nitrogen compounds in the bio-oil produced [8]. **Figure 6 (c)** shows that the nitrogenous compounds present in bio-oil do not have an ordered spatial organization.

The 56 peaks of nitrogen compounds found in the bio-oil include pyridines, pyrroles, indoles, amines and nitriles. Pyridine has pharmaceutical significance and is rarely found in its pure form. Industrially it is obtained from coal tar but is only available in small amounts (approximately 0.1%).

The literature provides limited information on the specific and global composition of the bio-oil produced by cottonseed pyrolysis. Apaydin-Varol et al., [25] performed fast pyrolysis of cottonseed and tentatively identified the chemical composition of the resulting bio-oil using GC / MS . The major compounds identified were: palmitic acid, linoleic acid, phenolic (4-methyl phenol) and nitrogenous compounds (1H Indol) and mostly straight chain hydrocarbons distributed in the range of C_{12} to C_{28}, which is similar to findings obtained in transport fuels. S. Seal et al., [58] performed the chemical characterization of the liquid product of cottonseed pyrolysis using GC-MS, identifying n-hexadecanoic acid as the most abundant compound, and noting the presence of a large number of organic compounds, such as hydrocarbons, organic acids, ketone and phenol, in addition to a minor amount of alkanes (>C10).

The use of GC×GC/TOF-MS associated with LTPRI software tools and dispersion plots performed in the present study, allowed for a comprehensive characterization of the global composition of cottonseed bio-oil. This classification increases the accuracy of compound identification and the reliability of the results, which are crucial for further

604 studies and for the development of biorefineries to process cottonseed residue for use
605 in several industrial applications.

606 **4. CONCLUSIONS**

607 Cottonseed bio-oil demonstrated a richness of nitrogen compounds which is not often
608 found in other types of bio-oil. This characteristic enhances the potential of this bio-oil
609 as a substitute for fossil fuel compounds that are difficult to obtain industrially.
610 Additionally, one of the major groups of compounds identified in the bio-oil were
611 phenolic compounds, which have important applications in a variety of fields, with the
612 major compound (phenol) being especially used in the production of phenolic resins.
613 In addition to nitrogenous and phenolic compounds, cottonseed bio-oil contained large
614 amounts of fatty acids and other organic compounds that could be transformed into
615 important raw materials. Fatty acids are useful for the production of biodiesel, while
616 hydrocarbons may be used as alternative fuels to petroleum derivatives and
617 oxygenated compounds (ketones, phenols) can be used as raw materials for fine
618 chemical engineering in the pharmaceutical, food and chemical industry.
619 The biochar obtained in the pyrolysis process and submitted to chemical activation
620 (K_2CO_3) possesses great potential as an adsorbent and generated surprising results
621 with regards to its high surface area and adsorption capacity. The application of
622 mathematical models to the adsorption results showed that the Langmuir isotherm
623 provided the best fit to the experimental data of all tests, indicating that the adsorption
624 of methylene blue dye by the activated biochar occurs mainly at the monolayer surface.
625

5. ACKNOWLEDGEMENTS

The authors would like to thanks the support of *Brazilian Coordenação de Aperfeiçoamento de Pessoal de Nível Superior (CAPES,* scholarships) and EBW+ Project Euro-Brazilian Windows Erasmus Mundus Program for the financial support of this work.

6. SUPPLEMENTARY MATERIAL DATA

The results and discussion for the Thermal gravimetric analysis, Proximate and Elemental analysis, Infrared Spectroscopy (FTIR), Scanning Electron Microscope (SEM), N_2-BET Adsorption Isotherms and Determination of pH at the point of zero charge (pH_{PZC}) with the respective references included, can be viewed in the **Supplementary Material Part A** and the complete list of compounds identified by GC×GC/TOFMS is presented in **Table B1 (Supplementary Material – Part B).**

7. REFERENCES

[1] Acikgoz C, Kockar OM. Characterization of slow pyrolysis oil obtained from linseed (Linum usitatissimum L.). J Anal Appl Pyrolysis 2009;85:151–4.

[2] Dhyani V, Bhaskar T. A comprehensive review on the pyrolysis of lignocellulosic biomass. Renew Energy 2018;129:695–716.

[3] Wang S, Dai G, Yang H, Luo Z. Lignocellulosic biomass pyrolysis mechanism: a state-of-the-art review. Prog Energy Combust Sci 2017;62:33–86.

[4] McKendry P. Energy production from biomass (part 1): overview of biomass. Bioresour Technol 2002;83:37–46.

[5] Kan T, Strezov V, Evans TJ. Lignocellulosic biomass pyrolysis: A review of product properties and effects of pyrolysis parameters. Renew Sustain Energy Rev 2016;57:1126–40.

[6] Singh R, Krishna BB, Mishra G, Kumar J, Bhaskar T. Strategies for selection of thermo-chemical processes for the valorisation of biomass. Renew Energy 2016;98:226–37.

[7] Alcalá A, Bridgwater A V. Upgrading fast pyrolysis liquids: Blends of biodiesel and pyrolysis oil. Fuel 2013;109:417–26.

[8] Hernandez E. Cottonseed 2016.

[9] Bellaloui N, Stetina SR, Turley RB. Cottonseed protein, oil, and mineral status in near-isogenic Gossypium hirsutum cotton lines expressing fuzzy/linted and fuzzless/linted seed phenotypes under field conditions. Front Plant Sci 2015;6:137.

[10] Primaz CT, Schena T, Lazzari E, Caramão EB, Jacques RA. Influence of the temperature in the yield and composition of the bio-oil from the pyrolysis of spent coffee grounds: Characterization by comprehensive two dimensional gas chromatography. Fuel 2018;232:572–80.

[11] Brunauer S, Emmett PH, Teller E. Adsorption of gases in multimolecular layers. J Am Chem Soc 1938;60:309–19.

[12] Barrett EP, Joyner LG, Halenda PP. The determination of pore volume and area distributions in porous substances. I. Computations from nitrogen isotherms. J Am Chem Soc 1951;73:373–80.

[13] Noh JS, Schwarz JA. Estimation of the point of zero charge of simple oxides by mass titration. J Colloid Interface Sci 1989;130:157–64.

[14] Reymond JP, Kolenda F. Estimation of the point of zero charge of simple and mixed oxides by mass titration. Powder Technol 1999;103:30–6.

[15] Jin H, Capareda S, Chang Z, Gao J, Xu Y, Zhang J. Biochar pyrolytically produced from municipal solid wastes for aqueous As (V) removal: adsorption property and its improvement with KOH activation. Bioresour Technol 2014;169:622–9.

[16] Maciel GP da S, Lazzari E, Bjerk TR, Ahmad SM, Carvalho APB de, Nogueira JMF, et al. Trace analysis of carbazole in commercial diesel by using adsorption

681 on activated biochar from rice husk pyrolysis. Int J Eng Res Sci (IJOER)[Recurso
682 Eletrônico] Bikaner, India Vol 3, No 8 (Aug 2017), p 46-57 2017.

683 [17] de Caprariis B, De Filippis P, Hernandez AD, Petrucci E, Petrullo A, Scarsella
684 M, et al. Pyrolysis wastewater treatment by adsorption on biochars produced by
685 poplar biomass. J Environ Manage 2017;197:231–8.

686 [18] Van den Dool H. A generalization of the retention index system including linear
687 temperature programmed gas-liquid partition chromatography. J Chromatogr A
688 1963;11:463–71.

689 [19] Von Mühlen C, Marriott PJ. Retention indices in comprehensive two-dimensional
690 gas chromatography. Anal Bioanal Chem 2011;401:2351–60.

691 [20] Cardoso CAL, Machado ME, Caramão EB. Characterization of bio-oils obtained
692 from pyrolysis of bocaiuva residues. Renew Energy 2016;91:21–31.

693 [21] Torri IDV, Paasikallio V, Faccini CS, Huff R, Caramão EB, Sacon V, et al. Bio-oil
694 production of softwood and hardwood forest industry residues through fast and
695 intermediate pyrolysis and its chromatographic characterization. Bioresour
696 Technol 2016;200:680–90.

697 [22] Jahirul MI, Rasul MG, Chowdhury AA, Ashwath N. Biofuels production through
698 biomass pyrolysis—a technological review. Energies 2012;5:4952–5001.

699 [23] Kelkar S, Saffron CM, Chai L, Bovee J, Stuecken TR, Garedew M, et al. Pyrolysis
700 of spent coffee grounds using a screw-conveyor reactor. Fuel Process Technol
701 2015;137:170–8.

702 [24] Al Afif R, Anayah SS, Pfeifer C. Batch pyrolysis of cotton stalks for evaluation of
703 biochar energy potential. Renew Energy 2020;147:2250–8.

704 [25] Apaydin-Varol E, Uzun BB, Önal E, Pütün AE. Synthetic fuel production from
705 cottonseed: fast pyrolysis and a TGA/FT-IR/MS study. J Anal Appl Pyrolysis
706 2014;105:83–90.

707 [26] Pütün AE, Özbay N, Önal EP, Pütün E. Fixed-bed pyrolysis of cotton stalk for
708 liquid and solid products. Fuel Process Technol 2005;86:1207–19.

709 [27] Bedmutha R, Booker CJ, Ferrante L, Briens C, Berruti F, Yeung KK-C, et al.
710 Insecticidal and bactericidal characteristics of the bio-oil from the fast pyrolysis
711 of coffee grounds. J Anal Appl Pyrolysis 2011;90:224–31.

712 [28] Zhang L, Liu R, Yin R, Mei Y. Upgrading of bio-oil from biomass fast pyrolysis in
713 China: A review. Renew Sustain Energy Rev 2013;24:66–72.

714 [29] Onorevoli B, Machado ME, Dariva C, Franceschi E, Krause LC, Jacques RA, et
715 al. A one-dimensional and comprehensive two-dimensional gas chromatography
716 study of the oil and the bio-oil of the residual cakes from the seeds of Crambe
717 abyssinica. Ind Crops Prod 2014;52:8–16.

718 [30] Yin R, Liu R, Mei Y, Fei W, Sun X. Characterization of bio-oil and bio-char
719 obtained from sweet sorghum bagasse fast pyrolysis with fractional condensers.
720 Fuel 2013;112:96–104.

721 [31] Garcia-Perez M, Wang XS, Shen J, Rhodes MJ, Tian F, Lee W-J, et al. Fast
722 pyrolysis of oil mallee woody biomass: effect of temperature on the yield and
723 quality of pyrolysis products. Ind Eng Chem Res 2008;47:1846–54.

724 [32] Czernik S, Bridgwater A V. Overview of applications of biomass fast pyrolysis
725 oil. Energy & Fuels 2004;18:590–8.
726 [33] Duman G, Okutucu C, Ucar S, Stahl R, Yanik J. The slow and fast pyrolysis of
727 cherry seed. Bioresour Technol 2011;102:1869–78.
728 [34] Vispute TP, Huber GW. Production of hydrogen, alkanes and polyols by aqueous
729 phase processing of wood-derived pyrolysis oils. Green Chem 2009;11:1433–
730 45.
731 [35] Gobi K, Mashitah MD, Vadivelu VM. Adsorptive removal of methylene blue using
732 novel adsorbent from palm oil mill effluent waste activated sludge: equilibrium,
733 thermodynamics and kinetic studies. Chem Eng J 2011;171:1246–52.
734 [36] Foo KY, Hameed BH. Insights into the modeling of adsorption isotherm systems.
735 Chem Eng J 2010;156:2–10.
736 [37] Hameed BH, Tan IAW, Ahmad AL. Adsorption isotherm, kinetic modeling and
737 mechanism of 2, 4, 6-trichlorophenol on coconut husk-based activated carbon.
738 Chem Eng J 2008;144:235–44.
739 [38] Weber K, Quicker P. Properties of biochar. Fuel 2018;217:240–61.
740 [39] Chandra TS, Mudliar SN, Vidyashankar S, Mukherji S, Sarada R, Krishnamurthi
741 K, et al. Defatted algal biomass as a non-conventional low-cost adsorbent:
742 surface characterization and methylene blue adsorption characteristics.
743 Bioresour Technol 2015;184:395–404.
744 [40] Nasrullah A, Bhat AH, Naeem A, Isa MH, Danish M. High surface area
745 mesoporous activated carbon-alginate beads for efficient removal of methylene
746 blue. Int J Biol Macromol 2018;107:1792–9.
747 [41] Hassan AF, Abdel-Mohsen AM, Fouda MMG. Comparative study of calcium
748 alginate, activated carbon, and their composite beads on methylene blue
749 adsorption. Carbohydr Polym 2014;102:192–8.
750 [42] Rangabhashiyam S, Anu N, Nandagopal MSG, Selvaraju N. Relevance of
751 isotherm models in biosorption of pollutants by agricultural byproducts. J Environ
752 Chem Eng 2014;2:398–414.
753 [43] Angın D, Altintig E, Köse TE. Influence of process parameters on the surface
754 and chemical properties of activated carbon obtained from biochar by chemical
755 activation. Bioresour Technol 2013;148:542–9.
756 [44] Foo KY, Hameed BH. Adsorption characteristics of industrial solid waste derived
757 activated carbon prepared by microwave heating for methylene blue. Fuel
758 Process Technol 2012;99:103–9.
759 [45] Gouamid M, Ouahrani MR, Bensaci MB. Adsorption equilibrium, kinetics and
760 thermodynamics of methylene blue from aqueous solutions using date palm
761 leaves. Energy Procedia 2013;36:898–907.
762 [46] Liu P, Liu W-J, Jiang H, Chen J-J, Li W-W, Yu H-Q. Modification of bio-char
763 derived from fast pyrolysis of biomass and its application in removal of
764 tetracycline from aqueous solution. Bioresour Technol 2012;121:235–40.
765 [47] Zaini MAA, Zakaria M, Setapar SHM-, Che-Yunus MA. Sludge-adsorbents from
766 palm oil mill effluent for methylene blue removal. J Environ Chem Eng

767 2013;1:1091–8.

768 [48] Cazetta AL, Vargas AMM, Nogami EM, Kunita MH, Guilherme MR, Martins AC,
769 et al. NaOH-activated carbon of high surface area produced from coconut shell:
770 Kinetics and equilibrium studies from the methylene blue adsorption. Chem Eng
771 J 2011;174:117–25.

772 [49] Fernandez ME, Nunell GV, Bonelli PR, Cukierman AL. Activated carbon
773 developed from orange peels: Batch and dynamic competitive adsorption of
774 basic dyes. Ind Crops Prod 2014;62:437–45.

775 [50] Foo KY, Hameed BH. Preparation, characterization and evaluation of adsorptive
776 properties of orange peel based activated carbon via microwave induced K2CO3
777 activation. Bioresour Technol 2012;104:679–86.

778 [51] Foo KY, Hameed BH. Preparation of activated carbon from date stones by
779 microwave induced chemical activation: Application for methylene blue
780 adsorption. Chem Eng J 2011;170:338–41.

781 [52] Deng H, Li G, Yang H, Tang J, Tang J. Preparation of activated carbons from
782 cotton stalk by microwave assisted KOH and K2CO3 activation. Chem Eng J
783 2010;163:373–81.

784 [53] Lazzari E, Schena T, Primaz CT, da Silva Maciel GP, Machado ME, Cardoso
785 CAL, et al. Production and chromatographic characterization of bio-oil from the
786 pyrolysis of mango seed waste. Ind Crops Prod 2016;83:529–36.

787 [54] Kim J-S. Production, separation and applications of phenolic-rich bio-oil–a
788 review. Bioresour Technol 2015;178:90–8.

789 [55] Bordoloi N, Narzari R, Sut D, Saikia R, Chutia RS, Kataki R. Characterization of
790 bio-oil and its sub-fractions from pyrolysis of Scenedesmus dimorphus. Renew
791 Energy 2016;98:245–53.

792 [56] Mamaeva A, Tahmasebi A, Tian L, Yu J. Microwave-assisted catalytic pyrolysis
793 of lignocellulosic biomass for production of phenolic-rich bio-oil. Bioresour
794 Technol 2016;211:382–9.

795 [57] Moraes MSA, Migliorini MV, Damasceno FC, Georges F, Almeida S, Zini CA, et
796 al. Qualitative analysis of bio oils of agricultural residues obtained through
797 pyrolysis using comprehensive two dimensional gas chromatography with time-
798 of-flight mass spectrometric detector. J Anal Appl Pyrolysis 2012;98:51–64.

799 [58] Seal S, Panda AK, Kumar S, Singh RK. Production and characterization of bio
800 oil from cotton seed. Environ Prog Sustain Energy 2015;34:542–7.

801